ARL-TR-8121 ● SEP 2017

US Army Research Laboratory

# Stress and Displacement Analysis of Microreactors during Thermal and Vacuum Loading

by William Allmon and C Mike Waits

## NOTICES

### Disclaimers

The findings in this report are not to be construed as an official Department of the Army position unless so designated by other authorized documents.

Citation of manufacturer’s or trade names does not constitute an official endorsement or approval of the use thereof.

Destroy this report when it is no longer needed. Do not return it to the originator.

ARL-TR-8121 ● SEP 2017

US Army Research Laboratory

# Stress and Displacement Analysis of Microreactors during Thermal and Vacuum Loading

**by William Allmon and C Mike Waits**
*Sensors and Electron Devices Directorate, ARL*

# REPORT DOCUMENTATION PAGE

*Form Approved*
*OMB No. 0704-0188*



| 1. REPORT DATE *(DD-MM-YYYY)* | 2. REPORT TYPE | 3. DATES COVERED (From - To) |
|---|---|---|
| September 2017 | Technical Report | 1 Dec 2016–30 June 2017 |

**4. TITLE AND SUBTITLE**
Stress and Displacement Analysis of Microreactors during Thermal and Vacuum Loading

**5a. CONTRACT NUMBER**

**5b. GRANT NUMBER**

**5c. PROGRAM ELEMENT NUMBER**

**6. AUTHOR(S)**
William Allmon and C Mike Waits

**5d. PROJECT NUMBER**

**5e. TASK NUMBER**

**5f. WORK UNIT NUMBER**

**7. PERFORMING ORGANIZATION NAME(S) AND ADDRESS(ES)**
US Army Research Laboratory
ATTN: RDRL-SED-E
2800 Powder Mill Road
Adelphi, MD 20783-1138

**8. PERFORMING ORGANIZATION REPORT NUMBER**
ARL-TR-8121

**9. SPONSORING/MONITORING AGENCY NAME(S) AND ADDRESS(ES)**

**10. SPONSOR/MONITOR'S ACRONYM(S)**

**11. SPONSOR/MONITOR'S REPORT NUMBER(S)**

**12. DISTRIBUTION/AVAILABILITY STATEMENT**
Approved for public release; distribution unlimited.

**13. SUPPLEMENTARY NOTES**

**14. ABSTRACT**
Compact power sources with high energy and power densities are critical for many military applications. These applications span from personal or squad-level power sources for long-duration missions without resupply to unmanned air vehicles requiring only a few hours of running time. In the 10–100 W+ power range, battery technology is the best solution currently available, but higher-energy dense technologies are needed to augment batteries and extend the available energy density well beyond state-of-the-art battery technology. One way to approach this is to take advantage of the large energy content of hydrocarbons. Conversion efficiencies of only a few percent can provide comparable energy density to battery technology. One technology being pursued by the US Army Research Laboratory is combustion-based thermophotovoltaic power sources. Combustion can be used to convert fuel to heat a surface to temperatures above 500 °C. An emitter could be vacuum brazed to the heated surface. This assembly method creates stresses due to difference in the coefficient of thermal expansion of the materials. Additional stresses are introduced, since the exterior of the assembly operates at vacuum while the interior is at ambient pressure. This report provides an analysis of 2 approaches to manage the stresses in the assembly.

**15. SUBJECT TERMS**
thermophotovoltaic, TPV, microcombustion, microreactors, combustion, photonic crystal, emitter, stress analysis, vacuum brazing, vacuum, brazing

| 16. SECURITY CLASSIFICATION OF: | | | 17. LIMITATION OF ABSTRACT | 18. NUMBER OF PAGES | 19a. NAME OF RESPONSIBLE PERSON |
|---|---|---|---|---|---|
| a. REPORT | b. ABSTRACT | c. THIS PAGE | | | William Allmon |
| Unclassified | Unclassified | Unclassified | UU | 26 | 19b. TELEPHONE NUMBER (Include area code) (301) 394-0117 |

## Contents


List of Figures iv

1. Background 1

2. Introduction 2

3. Simulation 3

4. Software Setup 5

5. Results 8

6. Conclusion 16

7. Future Improvements 17

8. References 18

List of Symbols, Abbreviations, and Acronyms 19

Distribution List 20

## List of Figures


Fig. 1 Primary components of the TPV energy converter[1] ..... 2
Fig. 2 MR 2.0.6 (dimensions in inches) ..... 3
Fig. 3 MR 2.0.6 detail view (dimensions in inches) ..... 4
Fig. 4 MR 2.1.4 (dimensions in inches) ..... 4
Fig. 5 MR 2.1.4 detail view (dimensions in inches) ..... 5
Fig. 6 Fixed surface during stress analysis ..... 6
Fig. 7 Mesh with 0.01-inch element size ..... 7
Fig. 8 Mesh close-up view ..... 8
Fig. 9 MR 2.0.6 and MR 2.1.4 stress ..... 9
Fig. 10 MR 2.0.6 stress due to thermal load ..... 9
Fig. 11 MR 2.0.6 stress due to thermal load cross sections ..... 10
Fig. 12 MR 2.1.4 stress due to thermal load ..... 11
Fig. 13 MR 2.1.4 stress due to thermal load cross sections ..... 11
Fig. 14 MR 2.0.6 and MR 2.1.4 stress above yield strength due to thermal loading only ..... 12
Fig. 15 Simulated displacement of MR 2.0.6 due to thermal load only ..... 13
Fig. 16 Comparison of simulated and measured displacement of MR 2.0.6 due to thermal load only ..... 14
Fig. 17 Simulated displacement of MR 2.1.4 due to thermal load only ..... 15
Fig. 18 Comparison of simulated and measured deformation of MR 2.1.4 due to thermal load only ..... 16

# 1. Background

Compact power sources with high energy and power densities are critical for many military applications. These applications span from personal or squad-level power sources for long-duration missions without resupply to unmanned air vehicles requiring only a few hours of running time. In the 10–100 W+ power range, battery technology is the best solution currently available. But higher-energy dense technologies are needed to augment batteries and extend the available energy density well beyond state-of-the-art battery technology (140 W·h/kg for rechargeable lithium [Li]-ion technology).[1]

One way to approach this is to take advantage of the large energy content of hydrocarbons or alcohols. Conversion efficiencies of only a few percent can provide comparable energy density to battery technology with the added advantage of instant recharge. One technology being pursued by the US Army Research Laboratory (ARL) is combustion-based thermophotovoltaic (TPV) power sources including a microreactor and heat recuperator. Combustion can be used to convert fuel to heat a surface to temperatures above 500 °C.[1]

Figure 1 describes the primary components of a TPV system: a heat source (microreactor), an emitter, and a photovoltaic converter. The heat source supplies thermal energy to the emitter, which radiates the energy across a gap to the photovoltaic cell or an array of photovoltaic cells. The photovoltaic cell(s) then converts the thermal radiation to electrical energy, which can be delivered to a load or conditioning circuitry. Optical filters between the emitter and the photovoltaic cell (not included in Fig. 1), as well as the reflectors deposited on the backside of the photovoltaic cell, are also common components. The optical cavity between the emitter and photovoltaic cell is often held under vacuum to minimize conduction and convective heat transfer.[1] For the concept demonstrator being developed at ARL, the exterior of the microreactor will also be held at vacuum to minimize heat loss.

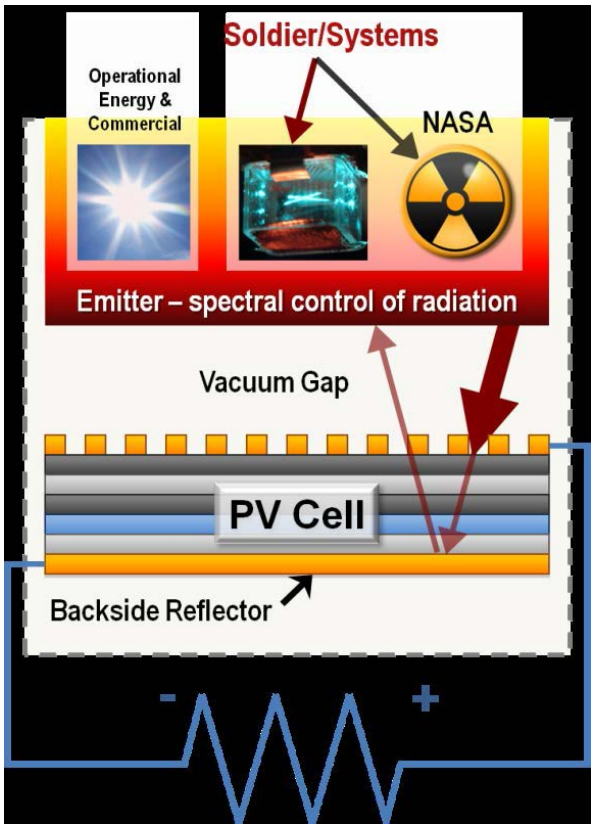


**Fig. 1 Primary components of the TPV energy converter[1]**

## 2. Introduction

Microreactor geometries consisting of 0.787- × 0.787-inch planar channels with wall thicknesses of 0.020 inch to limit conduction are investigated. A tantalum (Ta) emitter could be vacuum brazed to the 2 planar outer surfaces of the microreactor. As mentioned earlier, the exterior of the microreactor operates at vacuum. This assembly has 2 issues: 1) the difference in the coefficient to thermal expansion (CTE) causes deformation during cooling following brazing, greatly altering the channel gap, and 2) the pressure difference across the thin microreactor wall and emitter can permanently deform due to the high temperatures during combustion.

During sustained combustion in an Inconel 600 microreactor without an emitter, a bulge in the outer channel on both sides of the microreactor was observed. The bulge is caused by the stress induced by a greater than 1-atm pressure difference caused by operating in the vacuum environment and weakening of the Inconel at high temperatures.[2] A peak displacement of 0.040 inch was measured in the central region of the microreactor suggesting the outer channel heights on both sides each increase from 0.020 inch to 0.040 inch. This change can affect the heat exchanged from the walls to and from the gas and may in turn affect the coupling between the

heterogeneous and homogeneous reactions if the reactions are not completed in the inner channel.[3] Approaches to strengthen the outer microreactor walls are required to maintain the geometry integrity and may include adding in a rib structure or thickening the outer Inconel wall.[4] This report provides an analysis of these 2 approaches by simulating the stress and displacement due to thermal loading caused by brazing and vacuum loading due to the pressure difference between the interior and exterior of the microreactor.

## 3. Simulation

One version of the microreactor, designated Microreactor 2.0 with Rib, is fabricated using electrical discharge machining to create narrow internal channels (Figs. 2 and 3). One end of the microreactor is closed off with a plate electron beam welded in place. The other end has a plenum and tubes also electron beam welded in place. The section view in Fig. 2 shows the wall dimensions and a 0.040-inch-wide rib used to support the large outer surfaces. Figure 3 shows the dimensions of the internal channels and walls. The microreactor is fabricated of Inconel 600. An emitter consisting of a patterned Ultra 76 Alloy (Ta 2.5%W from HC Starck) surface to spectrally match to the photovoltaic converter will be attached on the 2 large exterior surfaces of the microreactor.[5] Prior to operating with the emitter, unpatterned Ultra 76 Alloy plates were vacuum brazed to the 2 large surfaces of the Microreactor 2.0 with Rib. This assembly is designated MR 2.0.6.

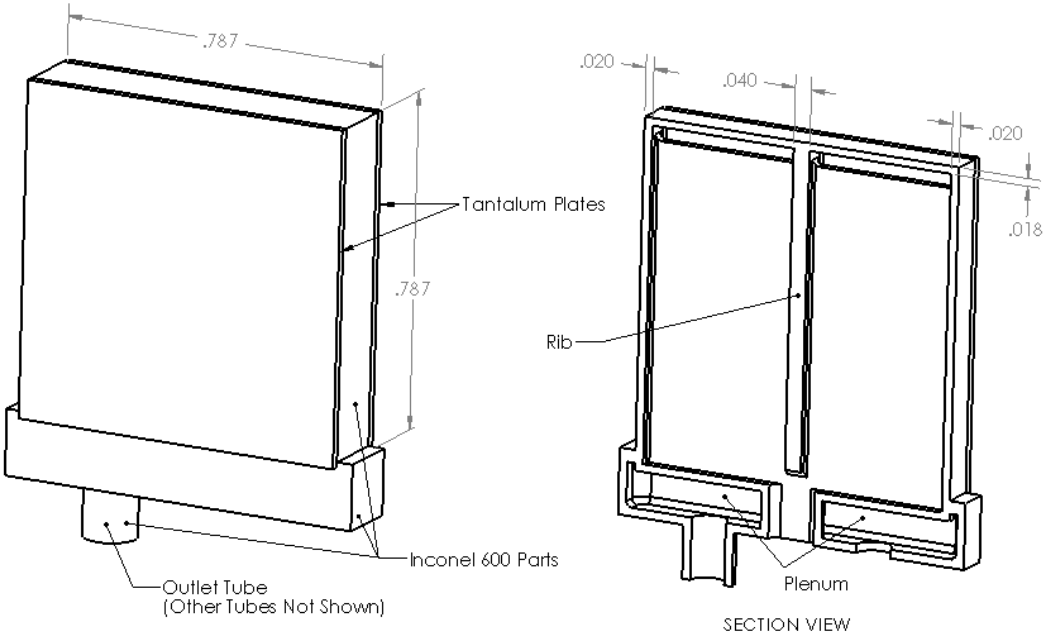


**Fig. 2 MR 2.0.6 (dimensions in inches)**

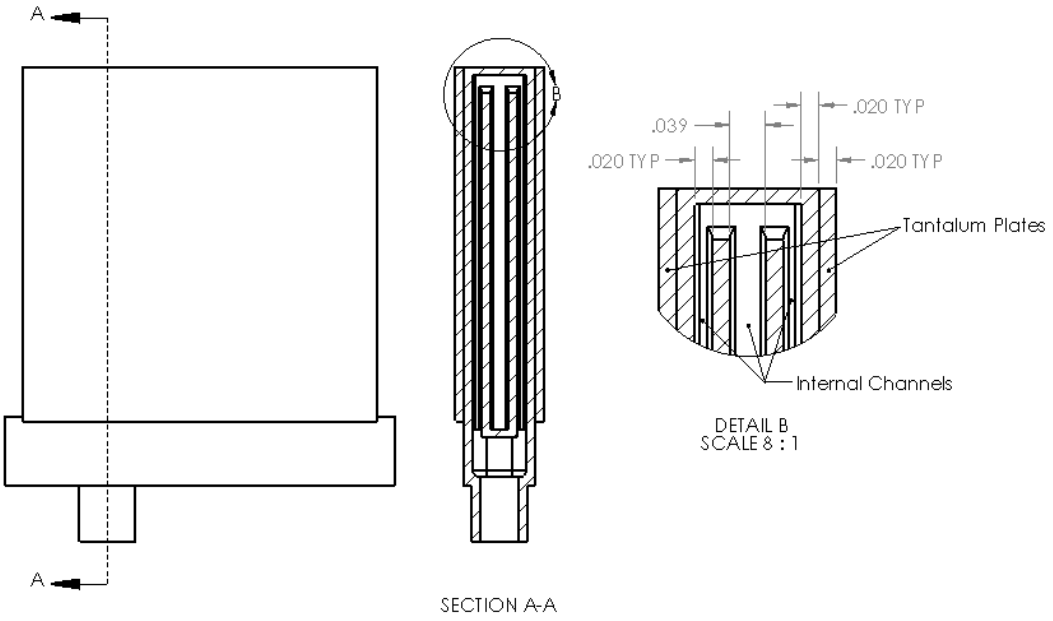


**Fig. 3 MR 2.0.6 detail view (dimensions in inches)**

Another microreactor, MR 2.1, is made of individual plates cut in various patterns, stacked together, and vacuum brazed to create internal channels. In contrast to MR 2.0.6, which has a rib, extra Inconel plates were vacuum brazed to the 2 large surfaces to add stiffness. Lastly, like MR 2.0.6, Ta plates were vacuum brazed to the 2 large surfaces. This assembly is designated MR 2.1.4. Figures 4 and 5 show the dimensions of the walls and internal channels.

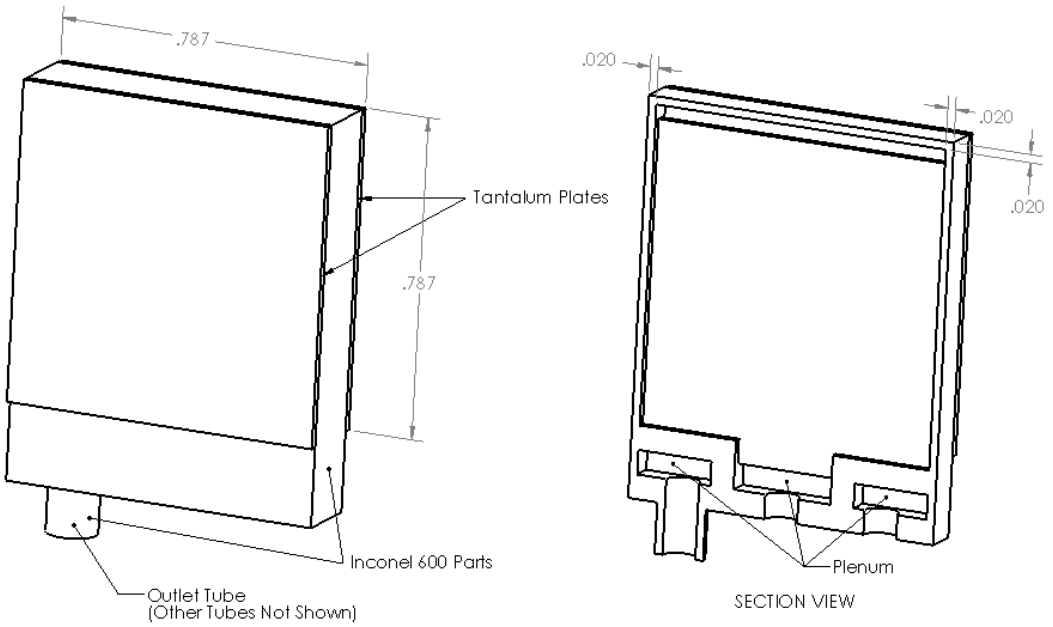


**Fig. 4 MR 2.1.4 (dimensions in inches)**

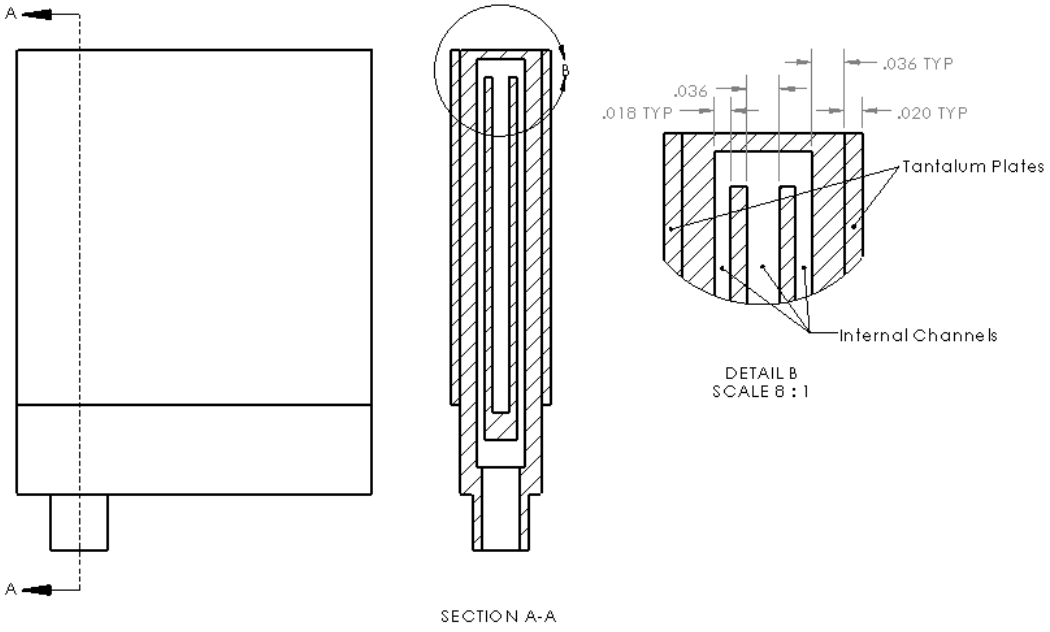


**Fig. 5 MR 2.1.4 detail view (dimensions in inches)**

This report shows the simulated stress and displacement of MR 2.0.6 and MR 2.1.4 due to thermal and vacuum loading, and compares the simulated displacement to the measured displacement in the actual assemblies. The joining of the Ta parts to the Inconel part through vacuum brazing occurs at approximately 1,100 °C. At this temperature, there are no stresses introduced, but as the assembly is cooled, stresses are introduced due to differences in the CTE. The worst case for our laboratory purposes occurs at room temperature where the largest temperature difference from the no stress condition occurs. In a field environment where the temperature may drop to –45 °C, the stresses will be even greater. In addition to stress due to this thermal loading, the exterior of the assembly is operated at vacuum while the internal channels are at approximately atmospheric pressure creating additional stresses in the assembly. The linear analysis was completed using SolidWorks Simulation.

## 4. Software Setup

This section details how the models were set up in SolidWorks Simulation. The analysis of the 2 microreactors were set up the same way. Symmetry of the geometry allowed half of the part to be modeled. The temperature at zero strain is set to 1,100 °C. This was the temperature when the microreactors and Ta plates were in their relax state prior to being joined through vacuum brazing. To run the stress portion of the simulation, a surface needed to be fixed to avoid rigid body

translation and/or rotation. A small portion of one of the tubes was added and a surface of this tube was fixed. These 2 steps were taken so as to have the least negative impact on the results. Figure 6 shows a small portion of a tube with a face of the tube fixed to enable the simulation to run. For the displacement portion of the analysis, this surface was not fixed and the Soft Springs feature in SolidWorks Simulation was used to stabilize the model. Using Soft Springs in the displacement case allowed a more realistic simulation without adding length to the tube, which would lengthen the analysis time.

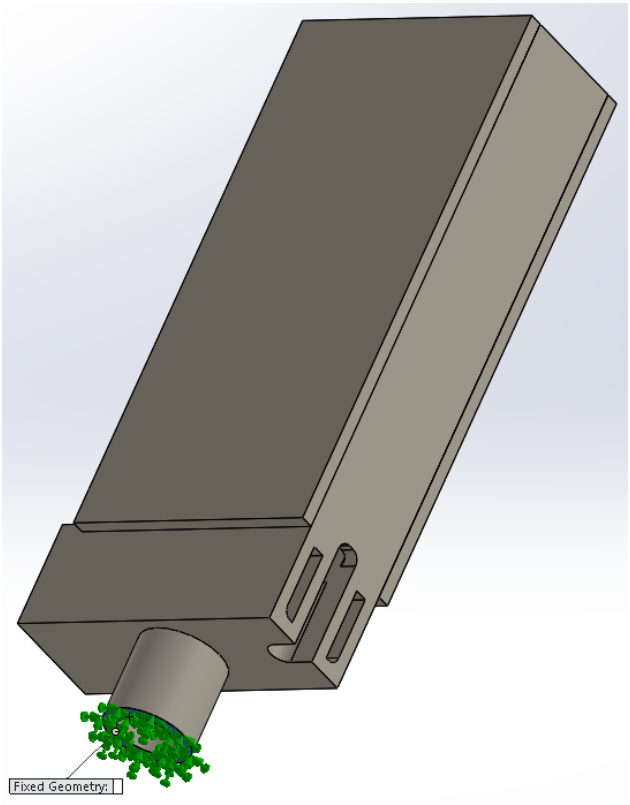


**Fig. 6 Fixed surface during stress analysis**

Three loading conditions were applied. Thermal load simulated the cooling from the brazing temperature of 1,100 to 25 °C by applying a thermal load of 25 °C. Thermal and vacuum load is the same as thermal load, but with the additional load of the exterior of the combustor at vacuum. Vacuum load simulates only the exterior of the combustor at vacuum. A mesh element size of 0.01 inch or smaller was selected for all cases. Table 1 shows the mesh details. Figures 7 and 8 show the mesh for an element size of 0.01 inch. Notice 2 elements characterize the Ta plate thickness.

**Table 1 Mesh details**

| Mesh Details | |
|---|---|
| Study name | Copy of [EDM Combustor 040 rib |
| Mesh type | Solid Mesh |
| Mesher Used | Standard mesh |
| Automatic Transition | Off |
| Include Mesh Auto Loops | Off |
| Jacobian points | 4 points |
| Element size | 0.01 in |
| Tolerance | 0.0005 in |
| Mesh quality | High |
| Total nodes | 458187 |
| Total elements | 293310 |
| Maximum Aspect Ratio | 8.4431 |
| Percentage of elements with Aspect Ratio < 3 | 99.9 |
| Percentage of elements with Aspect Ratio > 10 | 0 |
| % of distorted elements (Jacobian) | 0 |
| Remesh failed parts with incompatible mesh | Off |
| Time to complete mesh(hh:mm:ss) | 00:00:51 |

**Fig. 7 Mesh with 0.01-inch element size**

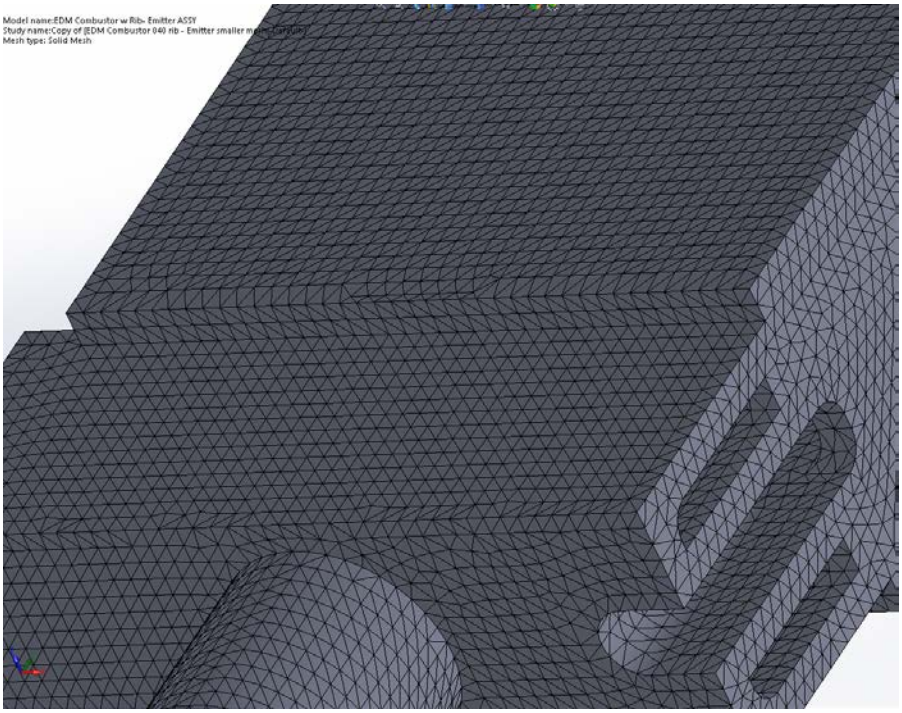


**Fig. 8 Mesh close-up view**

## 5. Results

Figure 9 shows the von Mises stress in MR 2.0.6 and MR 2.1.4 for the following 3 cases: thermal only, thermal and vacuum, and vacuum only. Notice there appears to be no difference in the stress between the thermal and thermal and vacuum cases. This makes sense since the maximum stress in the vacuum only case is less than 2.5 ksi, whereas in the thermal only and thermal and vacuum cases the stress is as high as 100 ksi. As a result, we look more carefully at the thermal only cases.

The CTE is $10.6 \times 10^{-6}$ cm/cm-°C for Inconel and $7.3 \times 10^{-6}$ cm/cm-°C for Ta at 25 °C. During the cooling of the assembly from the brazing temperature of 1,100 to 25 °C, the Inconel shrinks significantly more than the tantalum. Figures 10 and 11 show the stress in MR 2.0.6 due to thermal loading. From Fig. 10, the shrinkage of the 0.040-inch-wide Inconel rib creates high stress in the tantalum in the area over the rib (labeled A). The stress in the center of the rib is low (labeled B), since it is far away from the tantalum and the rib is thick compared to the Ta plates acting on it. The stress in the tantalum near the edge labeled C (shown in green) is not as high as the area labeled A since the Inconel pulling on it is not as thick as the rib and the edge of the tantalum is not fixed. In this same area, one can see a small line of yellow indicating higher stress where the tantalum contacts the Inconel. The stress in the Inconel in the area labeled D is high since the Inconel in this area is

only 0.020 inch thick (there is a reactor channel behind this area), deforms in a concave fashion due to the presence of the edges of the 2 Ta plates, and the nearby shrinkage of the 2 internal Inconel walls that create the reactor channels. Label D in Fig. 10a shows how the inner walls pulling on the Inconel in the area labeled D in Fig. 10. The area labeled E does not have the high stress area since the internal walls to not attach to the inside surface of this area. In Fig. 10, the area labeled F has high stress since it is being pulled from 2 directions. In the area labeled G in Fig. 10, the stress is low since this area is away from the rib and the edges of the assembly. The stress in the area labeled H is not quite as low as G since it is closer to the plenum area where there is a great deal of Inconel pulling on the tantalum. As expected, there is minimal stress in the Inconel in the area near the tube and the plenum where there is no Ta resisting the shrinkage of the Inconel.

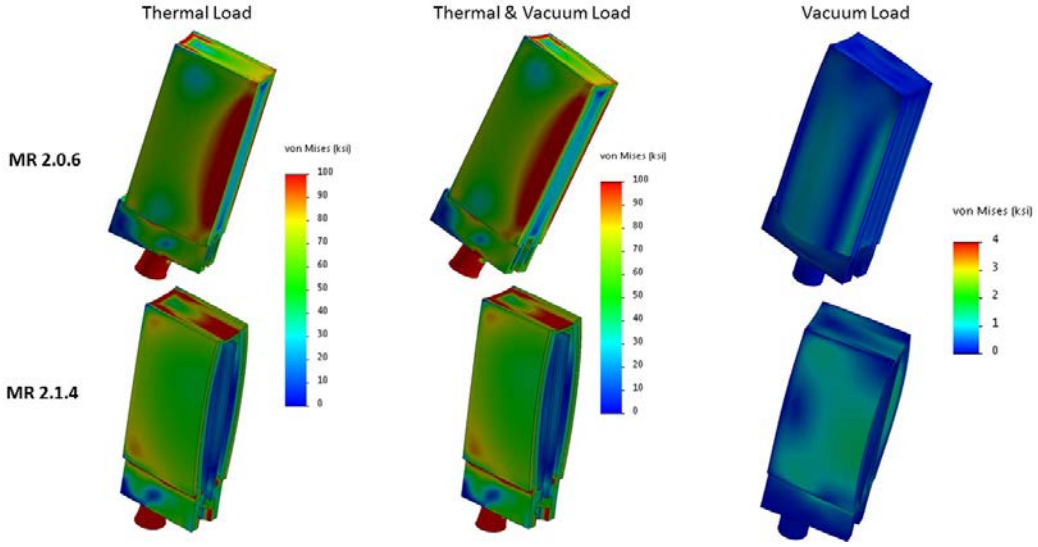


**Fig. 9 MR 2.0.6 and MR 2.1.4 stress**

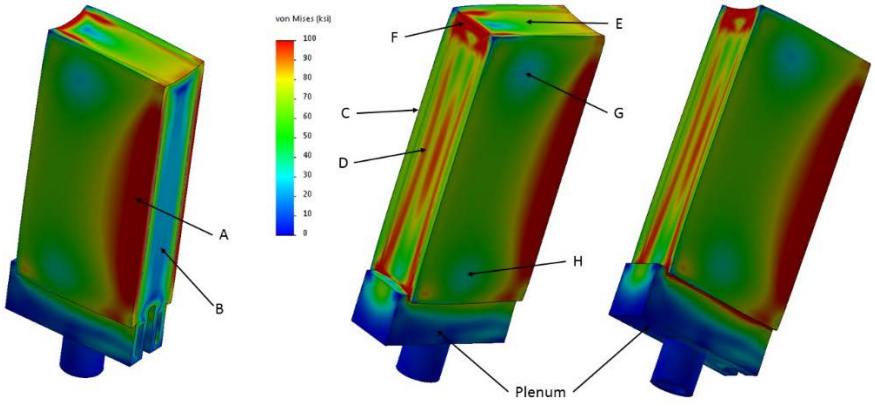


**Fig. 10 MR 2.0.6 stress due to thermal load**

From Fig. 11, the cross section of the assembly shows a high stress in the Inconel opposite of the high stress area in the tantalum (see Fig. 11a and b). The high stress area is smaller in the Inconel than in the tantalum due to the rib. The stress in the rib itself is not nearly as high since it is twice as thick. While in Fig. 11 it looks like the rib and the outer wall are the same thickness, recall the model was reduced in size through symmetry thus the rib is actually twice as thick. There is a particularly high stress in the Inconel in the area of the fillet near the rib as one can see in comparing Fig. 11c to d, which have a scale up to 150 ksi. This is to be expected since there is a dramatic change in thickness of the Inconel is this area.

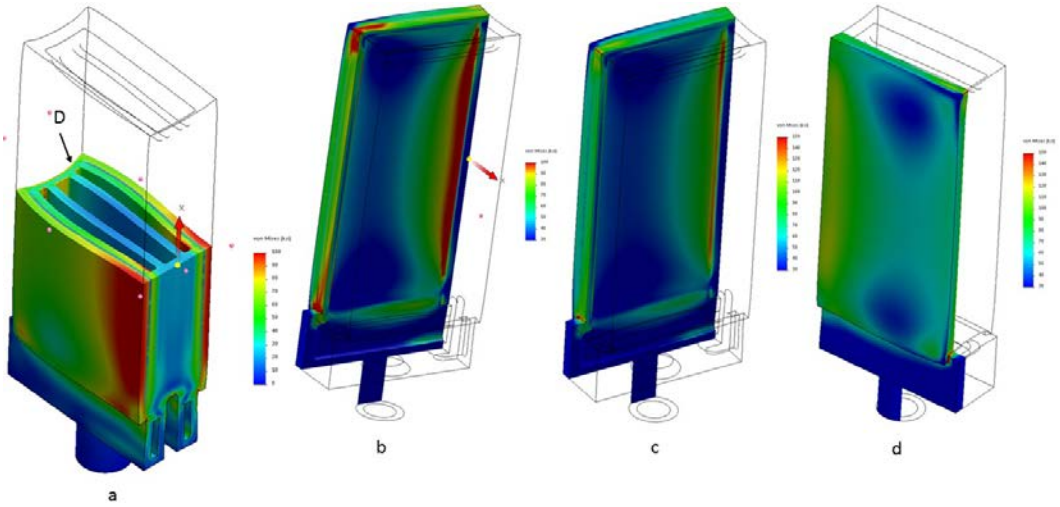


**Fig. 11 MR 2.0.6 stress due to thermal load cross sections**

Figures 12 and 13 show the stress in MR 2.1.4 due to thermal loading. From Fig. 12, one can see a high stress area of the tantalum is near the corner labeled A. This is likely due to the Inconel shrinking in 2 directions in this area. In contrast to MR 2.0.6, the center area of the tantalum in MR 2.1.4 has a lower stress since the outer Inconel wall is twice as thick. There is no rib to create this high-stress area. In Fig. 12, the stress in the tantalum near the edge labeled B (shown in green) is not as high as the area labeled A since the edge of the tantalum is not fixed. In this same area, one can see a small line of yellow indicating higher stress where the tantalum contacts the Inconel. The stress in the Inconel in the area labeled C is high since the Inconel is this area is only 0.020 inch thick and deforms in a concave fashion due to the presence of the edges of the 2 Ta plates and the shrinkage of the 2 internal Inconel walls that create the internal channels. Figure 13a and b shows how the inner walls pulling on the Inconel in the area labeled C in Fig. 12. The area labeled D has high stress since there is no rib to distribute the stress and the 2 Ta plates are acting on this surface. The area labeled E has high stress since it is being pulled from 2 directions. As expected, there is minimal stress in the Inconel in the area

near the tube and the plenum where there is no tantalum resisting the shrinkage of the Inconel.

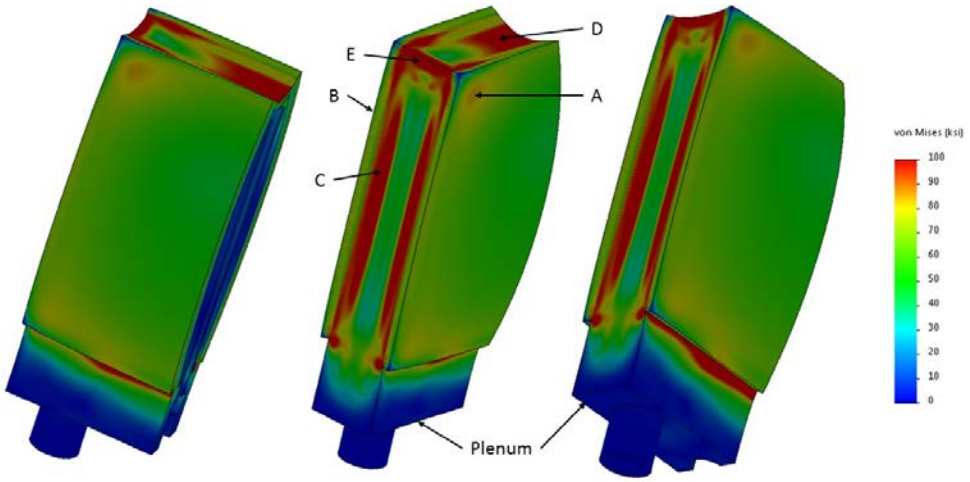


**Fig. 12 MR 2.1.4 stress due to thermal load**

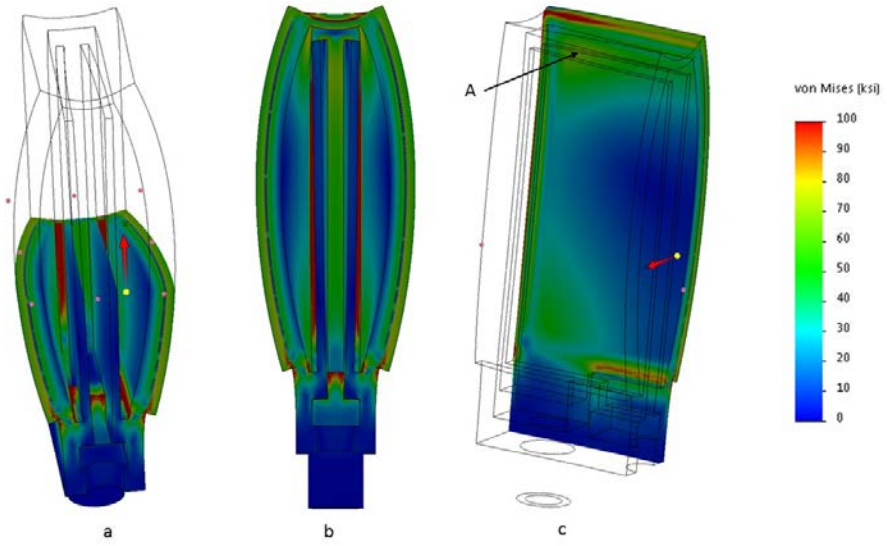


**Fig. 13 MR 2.1.4 stress due to thermal load cross sections**

From Fig. 13a and b, one can see the stress in the 2 internal walls that create the channels is low, as expected, since tantalum is not opposing its shrinkage. From Fig. 13c, the cross section of the assembly shows a high stress in the Inconel opposite of the high-stress area in the tantalum (see the area labeled A).

From Figs. 10–13, we can see many areas where the von Mises stress in the Inconel and Ta portions is greater than 100 ksi, which is well above the corresponding yield strength at 25 °C of 40[2] and 35 ksi, respectively. Figure 14 shows the areas of stress

for MR 2.0.6 and 2.14 that are over 40 ksi in red. This is a significant portion of the model. A more accurate solution can be obtained using a nonlinear analysis where the full stress-strain curves for the material can be specified. In comparing the analysis to the actual parts, we find the assembly is staying together and not peeling apart as may be predicted for materials bonded together experiencing such high stress.

Figure 15 shows the simulated resultant displacement of MR 2.0.6 due to thermal load only. The displacement ranges from 0 to 0.008 inch but the legend ranges from 0 to 0.006 since so little of the displacement is above 0.006 inch. The center area in blue shows a low displacement the center of the Ta plates is resisting the shrinkage of the Inconel. In contrast, the corner labeled A has a high displacement of 0.006 inch or more, since it is the edge of the Ta plates and the Inconel can become concaved in 2 planes. The area of the plenum away from the Ta plates (labeled B) has high displacement since the Inconel can shrink unopposed by the tantalum. Figure 15d, e, and f shows how the Inconel shrinks and become concave due to the Ta plates constraining this displacement. Recall these figures show only half of the reactor. The area labeled C has a displacement of 0.005 inch while the area labeled D has a displacement that ranges from 0.002 to 0.005 inch. The areas labeled C and D have less displacement since they can only become concave in one plane. The area labeled E shows minimal displacement while the edges show considerable shrinkage.

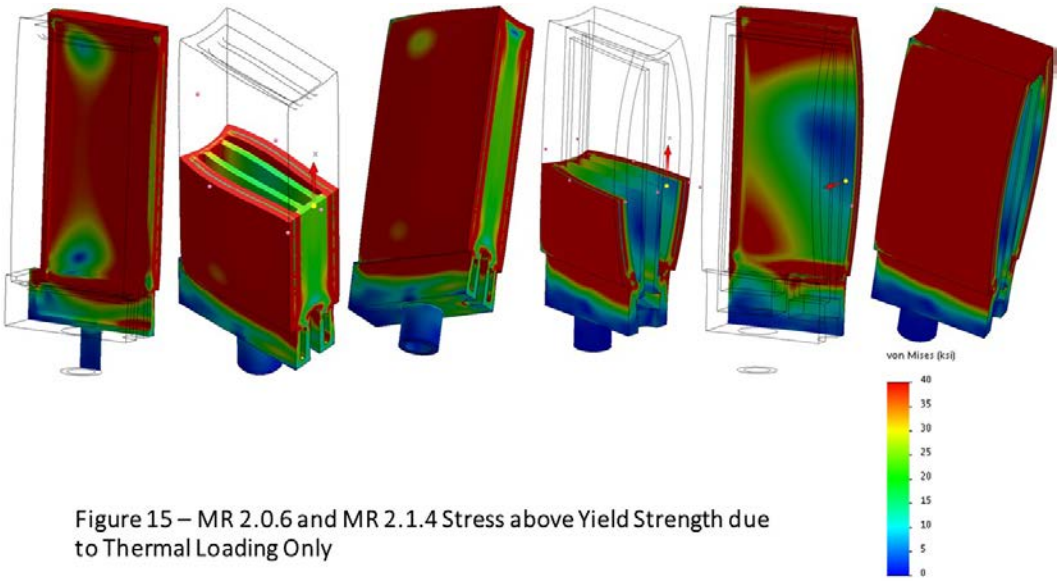


Figure 15 – MR 2.0.6 and MR 2.1.4 Stress above Yield Strength due to Thermal Loading Only

**Fig. 14 MR 2.0.6 and MR 2.1.4 stress above yield strength due to thermal loading only**

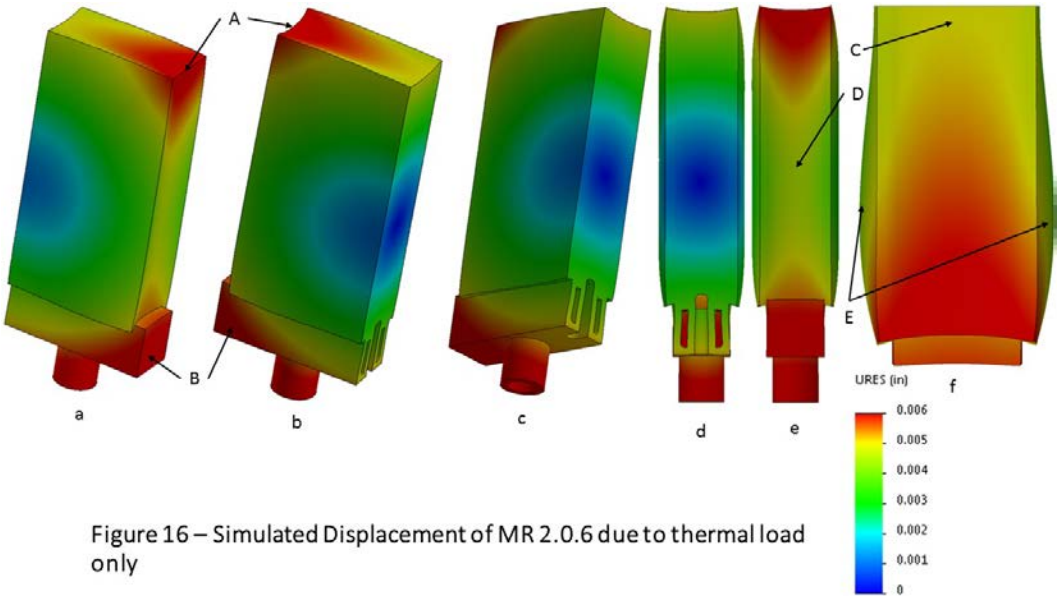


Figure 16 – Simulated Displacement of MR 2.0.6 due to thermal load only

**Fig. 15 Simulated displacement of MR 2.0.6 due to thermal load only**

Figure 16 compares the simulated displacement to the actual measure displacement of the MR 2.0.6 for the thermal loading only. The scale on the simulation case was changed to range from 0 to 0.005 inch. In the simulated case, the center area in blue shows minimal displacement. The displacement increases in areas the further from the center with a maximum of over 0.005 inch. For the actual reactors, all measurements are the variation in the z-direction (out of the paper) as a dial indicator followed horizontal and vertical paths shown by the lines on the combustor in these figures. The vertical paths showed a 0.005-inch variation and the horizontal paths showed a 0.002- to 0.005-inch variation. While the variations in the displacement are comparable between the simulation and the actual assembly, it is a difficult to judge if the location of the displacements is the same. In the measurements of the actual assembly, a datum needed to be established in the middle of the Ta plate, since the simulation predicts there was no or minimal displacement in this area. With this datum established, the displacement of various points on the Ta plate could be measured in the z-direction.

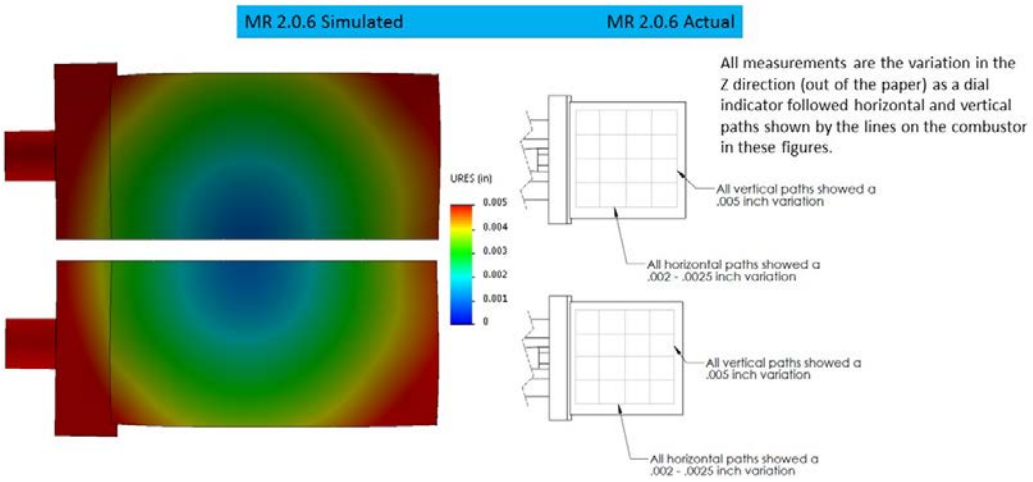


**Fig. 16 Comparison of simulated and measured displacement of MR 2.0.6 due to thermal load only**

Figure 17 shows the simulated resultant displacement of MR 2.1.4 due to thermal load only. The displacement ranges from 0 to 0.008 inch, but the legend ranges from 0 to 0.006 since so little of the displacement is above 0.006 inch. The only area with little to no displacement is the area in the near the center of the inner walls labeled A. On outer surface, the area marked B shown in light blue has a displacement of 0.001 to 0.002 inch. The majority of the rest of the Ta surface has a displacement of 0.002 to 0.004 inch, while the one corner has a displacement as high as 0.005 to 0.006 inch or more. The large displacement in the corner occurs since the edge of the Ta plates and the Inconel can become concaved in 2 planes. The area of the plenum away from the Ta plates (labeled C) has high displacement since the Inconel can shrink unopposed by the tantalum. Figure 17d and e shows how the Inconel shrinks and become concave due to the Ta plates constraining this displacement. Recall these figures show only half of the reactor. The area labeled D has a displacement of 0.005 inch, while the area labeled E has a displacement that ranges of 0.006 inch or greater. The area labeled F shows minimal displacement while the edges show considerable shrinkage.

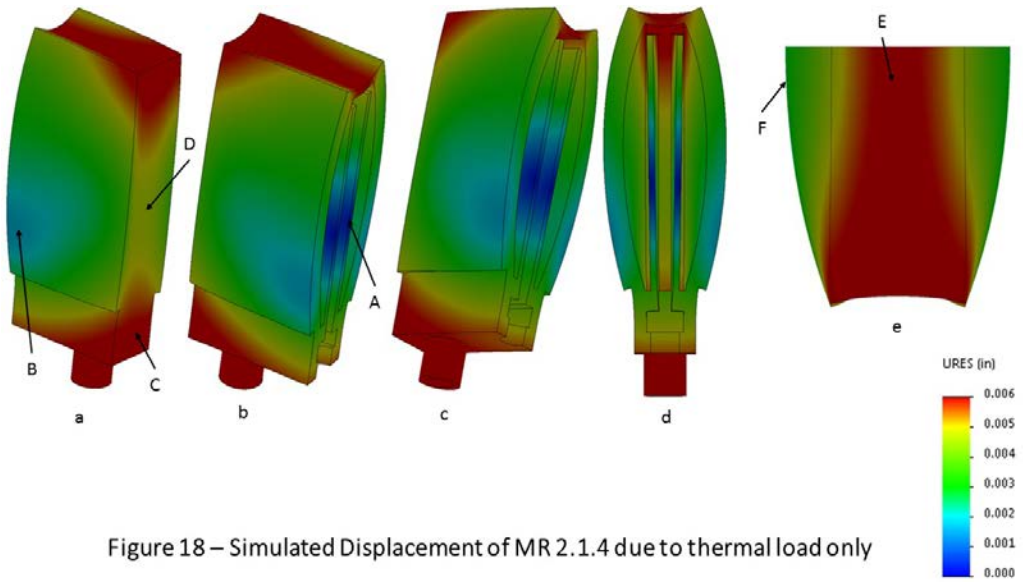


Figure 18 – Simulated Displacement of MR 2.1.4 due to thermal load only

**Fig. 17 Simulated displacement of MR 2.1.4 due to thermal load only**

Figure 18 compares the simulated displacement to the actual measure displacement of the MR 2.1.4 for the thermal loading only. The scale on the simulation case was changed to range from 0 to 0.005 inch. In the simulated case, the center area closer to the plenum shown in light blue has a displacement of 0.001 to 0.002 inch. The displacement increases in areas the further from the center with a maximum of over 0.005 inch. For the actual reactors, all measurements are the variation in the z-direction (out of the paper) as a dial indicator followed horizontal and vertical paths shown by the lines on the combustor in these figures. For side 1, there is a bubble shown by the ellipse. This bubble resulted in the vertical and horizontal paths through the center of the reactor measuring a variation of 0.015 to 0.017 inch. For the horizontal paths along the outer edges, the displacement variation measured 0.002 inch. Along the vertical paths on the outer edges, the displacement variation was 0.005 inch. For side 2, the vertical and horizontal paths through the center of the reactor showed a 0.005- to 0.006-inch variation. For the horizontal paths along the outer edges, the displacement ranges from 0.003 to 0.004 inch. Along the vertical paths on the outer edges, the displacement variation was 0.001 inch. Except for the bubble, the variations in the displacement are comparable between the simulation and the actual assembly, but it is a difficult to judge if the location of the displacements is the same. The bubble is mostly likely not caused by stress but as a result of surface contamination.[6] In the measurements of the actual assembly, a datum needed to be established in the area of the Ta plate predicted to have minimal displacement. With this datum established, the displacement of various points on the Ta plate could be measured in the z-direction.

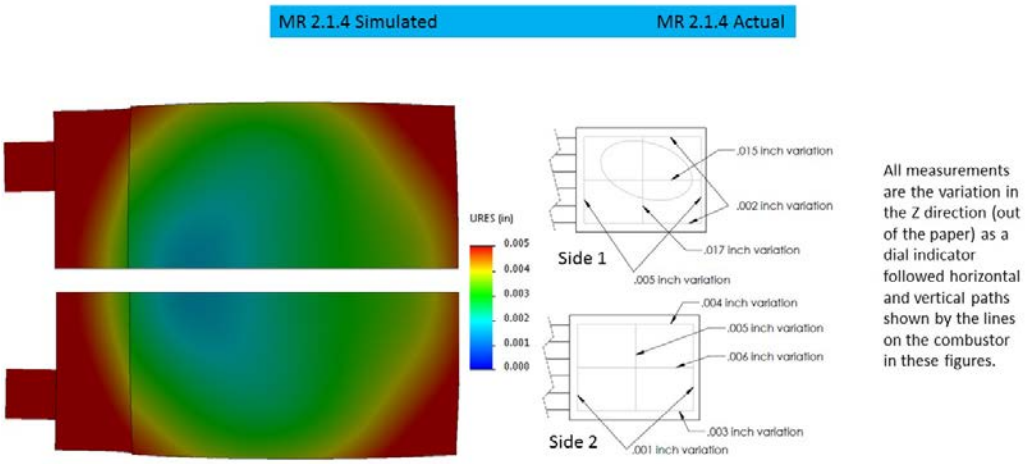


**Fig. 18 Comparison of simulated and measured deformation of MR 2.1.4 due to thermal load only**

## 6. Conclusion

This report shows the simulated stress and displacement of MR 2.0.6 and MR 2.1.4 due to thermal and vacuum loading, and compares the simulated displacement to the measured displacement in the actual assemblies. The joining of the Ta parts to the Inconel part through vacuum brazing occurs at approximately 1,100 °C. At this temperature, there are no stresses introduced, but as the assembly is cooled, stresses are introduced due to differences in the CTE. In addition to stress due to this thermal loading, the exterior of the assembly is operated at vacuum while the internal channels are at approximately atmospheric pressure, potentially creating additional stresses in the assembly.

From the analysis, the additional stress at room temperature due to the vacuum loading is minimal and can be ignored. In contrast, at room temperature, the simulated stresses due to the CTE mismatch in a large portion of the assembly are beyond the yield strength of both Inconel 600 and tantalum both in the annealed condition, 40[2] and 35[7] ksi, respectively. It is good design practice to stay inside the yield strength, which also ensures the displacements are minimal during loading and the design returns to its original shape after the load is removed. Aside from the yield strength, the simulation indicates the stresses in portions of the assembly are at or above the ultimate tensile strength of the materials, which are 80–100 ksi for annealed Inconel 600 sheet[2] and 50 ksi for the Ta sheet (Ultra 76 Alloy, Ta 2.5%W from HC Starck).[7] It is likely the residual stress has been released by the plastic deformation. This process has work hardened the material so it has a higher yield strength. Although no failures have occurred in the actual parts, potential failures include a pealing apart of the tantalum and Inconel or a crack in the Inconel,

which could lead to the loss of vacuum. A design with thicker Inconel walls would reduce the stress and displacement of the Inconel, but increase the stress in the tantalum. Another benefit to thickening the Inconel walls is the channel dimensions are more likely to be maintained thus reducing one of the myriad of variable in the combustion process. At the high operating temperatures, the vacuum loading may become a factor as the strength of the materials reduces. Another reason to increase the Inconel wall thickness and thus reduce the displacement is when the actual Ta emitter is brazed onto the microreactor, the displacement of the tantalum may alter the pattern on the surface leading to degraded emission performance. Unfortunately, thickening the walls may also affect the heat exchanged from the walls to and from the gas and may in turn affect the coupling between the heterogeneous and homogeneous reactions.[3]

Comparing Figs. 10 and 12, MR 2.0.6 appears to have higher stress in the tantalum compared to MR 2.1.4. Comparing Figs. 11 and 13, which show the Inconel surface opposite the Ta plates, MR 2.0.6 has higher stress in the Inconel compared to MR 2.1.4. These results indicate the added Inconel thickness of MR 2.1.4 design reduces stresses more than the rib of MR 2.0.6. A more accurate solution can be obtained using a nonlinear analysis where the full stress-strain curves for the material can be specified and the rupture point of the materials can be included.

## 7. Future Improvements

We suggest the following future improvements:

- Obtain a more accurate solution using a nonlinear analysis where the full stress-strain curves for the materials can be specified.
- Establish a datum plane as predicted by the simulation and use a coordinate measuring machine to take measurement at various points and create a map of the displacement.
- Cut the MR 2.1.4 through the area with the bubble to determine if this is a void or something else.
- Run temperature-dependent studies of microreactors without the zero strain condition at 1,100 °C to see if we can properly model stress and displacement due to vacuum and high temperature.
- Run simulations of microreactors with thicker Inconel walls to determine the increased stress in the tantalum.

## 8. References


1. Waits MC. Thermophotovoltaic energy conversion for personal power sources. Adelphi (MD): Army Research Laboratory (US); 2012 Feb. Report No.: ARL-TR-5942.

2. Inconel 600 datasheet. New Hartford (CT): Special Metals Corporation; 2008.

3. Tolmachoff ED, Allmon WR, Waits CM. Applied Energy. 2014;128:111–118

4. Waits CM, Tolmachoff ED, Allmon WR, Zecher-Freeman NE. Energy analysis of *n*-Dodecane combustion in a hetero/homogeneous heat-recirculating microreactor for portable power applications, power MEMS. Journal of Physics: Conference Series. 2016;773:012060.

5. Stelmakh V, Rinnerbauer V, Geil RD, Aimone PR, Senkevich JJ, Joannopoulos JD, Soljacˇic´M, Celanovic I. Appl Phys Lett. 2013;103:123903.

6. Kay D. Voids in brazen joints. Burlington (Canada): Vac Aero International; 2010 Jan 15 [accessed 2017]. https://vacaero.com/information-resources/vacuum-brazing-with-dan-kay/833-voids-in-brazed-joints.html.

7. Ultra 76 Alloy (Ta 2.5%W) datasheet. Munich (Germany): HC Starck; 2010, Number PD-7033, Issue 1-05.03.

## List of Symbols, Abbreviations, and Acronyms

| | |
|---|---|
| ARL | US Army Research Laboratory |
| CTE | coefficient of thermal expansion |
| Li | lithium |
| Ta | tantalum |
| TPV | thermophotovoltaic |

| | |
|---|---|
| 1 (PDF) | DEFENSE TECHNICAL INFORMATION CTR DTIC OCA |
| 2 (PDF) | DIR ARL RDRL CIO LL IMAL HRA MAIL & RECORDS MGMT |
| 1 (PDF) | GOVT PRINTG OFC A MALHOTRA |
| 2 (PDF) | ARL RDRL SED E W ALLMON CM WAITS |